In Silico Populations Optimized on Optogenetic Recordings Predict Drug Effects in Human Induced Pluripotent Stem Cell-Derived Cardiomyocytes

Michelangelo Paci[1], Elisa Passini[2], Aleksandra Klimas[3], Stefano Severi[4], Jari Hyttinen[1], Blanca Rodriguez[2], Emilia Entcheva[3]

[1]Faculty of Biomedical Sciences and Engineering, Tampere University of Technology, Tampere, Finland
[2]Department of Computer Science, University of Oxford, Oxford, United Kingdom
[3]Department of Biomedical Engineering, The George Washington University, Washington DC, United States of America
[4] Department of Electrical, Electronic and Information Engineering, University of Bologna, Cesena, Italy

Abstract

All-optical high-throughput systems allow simultaneous high resolution action potential (AP) and Ca^{2+} transient (CaTr) measurements from cardiomyocytes within multicellular context, offering means to speed up in vitro drug tests. Here, we aim to develop experimentally-constrained in silico models of human induced pluripotent stem cell-derived cardiomyocytes (hiPSC-CMs) and hiPSC-CM populations to predict drug effects in humans, by leveraging functional data obtained by all-optical means. Using multi-objective genetic algorithms (MoGAs), we constructed three control populations of in silico hiPSC-CMs, constrained with experimental data of APs and CaTrs recorded at room temperature and non-paced conditions from three different plates containing hiPSC-CM syncytia. We then simulated the effect of increasing doses of Diltiazem (130 models), Cisapride (200 models) and Astemizole (200 models) in the three populations, respectively. Comparing model predictions with the experimental drug administration (not used for the optimization/calibration of the populations) revealed good agreement with experiments: e.g. Diltiazem shortened APs while Astemizole and Cisapride prolonged APs.

1. Introduction

Optical approaches offer contact-free high-resolution measurements of key electromechanical parameters in cardiomyocytes, e.g. action potentials (AP), Ca^{2+} transients (CaTr), or contraction. Recently, all-optical high-throughput systems allowed simultaneous AP and CaTr measurements from cardiomyocytes within multicellular context, offering means to speed up *in vitro* drug tests [1,2]. In this work, we aim (i) to calibrate/optimize populations of *in silico* models of human induced pluripotent stem cell-derived cardiomyocytes (hiPSC-CMs) by means of simultaneous optically recorded data of APs and CaTrs in control conditions and (ii) to assess the predictive power of our *in silico* populations during the administration of three specific drugs (Diltiazem, Cisapride and Astemizole) plus a fourth drug (Dofetilide) as positive control.

2. Methods

2.1. Experimental dataset

The experimental dataset consists in APs and CaTrs optically recorded from hiPSC-CMs syncytia (CDI iCell^2 cardiomyocytes) at room temperature under non-paced conditions. Recordings were performed in control conditions and after administration of one of the following drugs: Diltiazem (mainly an I_{CaL} blocker), Cisapride and Astemizole (both mainly I_{Kr} blockers). In detail, recordings were performed on three plates (384-well format), where APs and CaTrs were recorded in negative control (administration of 0.1% DMSO, C-) and then administered with four increasing doses (D1, D2, D3 and D4) of Diltiazem (Plate 1), Cisapride (Plate 2) and Astemizole (Plate 3). Furthermore, 0.5 nM Dofetilide was tested on all the plates as positive control (C+). APs and CaTrs were recorded from five C- samples and from six samples each of C+, D1, D2, D3 and D4. Experimental biomarkers for the three plates are reported in Table 1. For each biomarker, we had five measurements in C- and six measurements in the other conditions. Biomarkers are: AP and CaTr cycle length (Vm CL and Ca CL), duration at 30%, 50% and 90% of AP (APD_{30}, APD_{50} and APD_{90}) and

 ISSN: 2325-887X DOI: 10.22489/CinC.2018.086

Table 1. Lower bounds (LB) and upper bounds (UB) for the five AP biomarkers and the six CaTr biomarkers for the three plates in C- conditions. Values in bold were computed as mean±2SD, values in italic were computed as mean±3SD, to be used in section 2.2.2.

	Plate 1		Plate 2		Plate 3	
	LB	UB	LB	UB	LB	UB
Vm CL (ms)	**4989**	**8423**	**2172**	**4255**	**3079**	**5222**
	4690	*9019*	*1842*	*4712*	*3003*	*5461*
APD_{90} (ms)	**786**	**1145**	**938**	**1116**	**831**	**1275**
	756	*1196*	*916*	*1142*	*721*	*1386*
APD_{50} (ms)	**520**	**752**	**736**	**910**	**698**	**921**
	504	*772*	*717*	*934*	*672*	*958*
APD_{30} (ms)	**391**	**575**	**515**	**673**	**459**	**719**
	377	*586*	*502*	*693*	*438*	*767*
Vm Tri90-30 (ms)	**393**	**571**	**418**	**478**	**253**	**564**
	369	*611*	*406*	*491*	*175*	*641*
Ca CL (ms)	**4997**	**8429**	**2174**	**4255**	**3084**	**5218**
	4701	*9028*	*1845*	*4711*	*3019*	*5455*
CTD_{90} (ms)	**904**	**2306**	**1564**	**2023**	**1434**	**2322**
	554	*2656*	*1541*	*2093*	*1310*	*2460*
CTD_{50} (ms)	**804**	**1163**	**979**	**1095**	**918**	**1149**
	751	*1194*	*972*	*1106*	*882*	*1178*
CTD_{30} (ms)	**644**	**903**	**828**	**903**	**761**	**931**
	615	*918*	*825*	*909*	*734*	*945*
Ca tRise (ms)	**221**	**373**	**331**	**413**	**286**	**443**
	196	*382*	*312*	*423*	*277*	*463*
Ca Tri90-30 (ms)	**258**	**1545**	**727**	**1121**	**667**	**1424**
	0	*1867*	*681*	*1186*	*567*	*1545*

of CaTr (CTD_{30}, CTD_{50}, CTD_{90}), AP and CaTr triangulation (Vm Tri90-30=APD_{90}-APD_{30} and Ca Tri90-30=CTD_{90}-CTD_{30}) and CaTr time to rise from 10% to 90% (Ca tRise). For each plate and biomarker, we considered as lower bounds (LB_i, $LB_{3SD,i}$) the smallest of mean-2SD and mean-3SD, while as upper bounds (UB_i, $UB_{3SD,i}$) the maximum of mean+2SDand mean+3SD of the five control measurements for the biomarker i (see Table 1, values in bold for ±2SD and in italic for ±3SD).

2.2. *In silico* modeling

2.2.1 Adapting the hiPSC-CM model to room temperature

Simulations were performed with the recently published Paci2018 hiPSC-CM model [3], which was tuned and validated to simulate APs and CaTrs at 37°C. To simulate the aforementioned experiments, we adapted the model to room temperature (21°C) by rescaling the model time constants for the main ionic currents according to the Q10 factors reported in Table 2.

Table 2. Q10 factors to translate the model from 37°C to 21°C [4–7].

Ionic current	Q10 factors
I_{Na}	2.00
I_{NaL}	2.20
I_{CaL}	2.10
I_f	4.50
I_{Kr} activation	4.55
I_{Kr} inactivation	3.08
I_{Ks}	2.00
I_{to}	2.00

2.2.2 Multi-objective genetic algorithms

Instead of a canonical approach to develop a population of *in silico* models, as in [8,9], here we opted for multi-objective genetic algorithms (MoGAs) [10]: they allow the concurrent optimization of many fitness functions, to find an optimal population. We chose to sample the following 22 parameters: (i) the maximum conductances/currents of I_{Na}, I_f, I_{CaL}, I_{to}, I_{Ks}, I_{Kr}, I_{K1}, I_{NCX}, I_{NaK}, I_{pCa}, I_{NaL}, I_{RyR}, I_{SERCA}; (ii) activation and inactivation time constants of I_{Na}, I_{CaL} and I_{RyR}; (iii) adaptation time constant and half inactivation Ca^{2+} concentration of I_{RyR}; (iv) I_{SERCA} half saturation constant. We defined two fitness functions, based on AP and CaTr biomarkers, respectively.

$$Err = \sum_{1}^{Nbiomarkers} err_i$$

$$err_i = \frac{(b_{i,sim} < LB_i)(b_{i,sim} - LB_i)^2 + (b_{i,sim} > UB_i)(b_{i,sim} - UB_i)^2}{0.5(LB_i + UB_i)},$$

where $b_{i,sim}$ is the i-th simulated biomarker, LB_i the i-th experimental lower bound for $b_{i,sim}$, UB_i the i-th experimental upper bound for $b_{i,sim}$ and Nbiomarkers the number of biomarkers computed on the experimental APs (5 biomarkers) and CaTrs (6 biomarkers). Shortly, if the simulated i-th biomarker is smaller than LB_i or greater than UB_i, the error is computed as the squared distance between the simulated biomarker and the bound, normalized by the center of mass of [LB_i, UB_i]. The biomarkers used to constrain the fitness functions are listed in Section 2.1 and Table 1. MoGAs parameters were: maximum number of models = 200 and maximum number of generations = 40. For each of the 200 parameter sets optimized by MoGAs, we then run the simulation up to steady state (500s) and re-checked that all the biomarkers were included in the ranges [$LB_{3SD,i}$, $UB_{3SD,i}$], to include in the population also those parameter sets at the very edge of the ranges [LB_i, UB_i].

2.2.3 Drug tests

To assess the predictive power of our three populations of hiPSC-CM models, we then simulated Diltiazem, Cisapride, Astemizole and Dofetile (C+) at the four doses

Table 3. IC_{50} and Hill's coefficients (in brackets) for the four drugs in rows 2-7 [11]. The experimentally tested drug doses are reported in µM in rows 8-12.

		Diltiazem	Cisapride	Astemizole	Dofetilide
Ionic currents	I_{Na}	22.4 (1.29)	333.7 (1)	3 (1.95)	162.1 (1)
	I_{Kr}	13.2 (1.16)	0.02 (1.04)	0.004 (0.78)	0.03 (1.2)
	I_{CaL}	0.76 (1.14)	11.8 (1)	1.1 (1.66)	26.7 (1)
Doses (µM)	C+	---	---	---	0.0005
	D1	0.01	0.0032	0.0001	---
	D2	0.1	0.01	0.001	---
	D3	1	0.0316	0.01	---
	D4	10	0.1	0.1	---

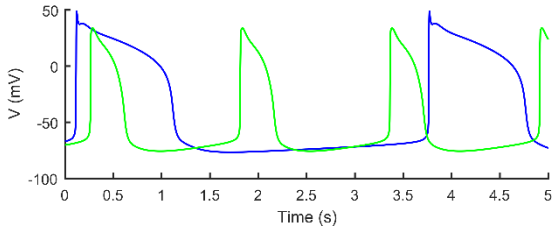

Figure 1. Spontaneous APs simulated by the Paci2018 model at 37°C (green) and 21°C (blue).

tested experimentally. Of note, the biomarkers computed on APs and CaTrs after drug administration were not used for the parameter set identification with MoGAs. Drug administration was simulated with the single pore block model on the three control populations, as in [8]. In Table 3 we reported the IC_{50} and the Hill's coefficients for the four drugs, together with the experimentally administered doses and the blocking effects on the ionic currents.

3. Results

Figure 1 compares the Paci2018 APs at 37°C and 21°C: as expected, the rate of spontaneous APs is slower and APD is longer at 21°C. This step helped also shifting AP and CaTr biomarkers closer to the experimental values recorded in C- conditions. MoGAs optimization produced three *in silico* control hiPSC-CMs populations, each representing the variability of a specific experimental plate. We then tested on each of these populations the corresponding drug which was tested experimentally. Specifically, Plate 1 (Diltiazem) contains 130 models, while Plate 2 (Cisapride) and Plate 3 (Astemizole) 200 models. Figure 2, 3 and 4 show the model distributions within the [LB_{3SD}, UB_{3SD}] variability intervals of the biomarkers in each plate. For each biomarker, simulations and experimental variability ranges are reported in C-, C+,

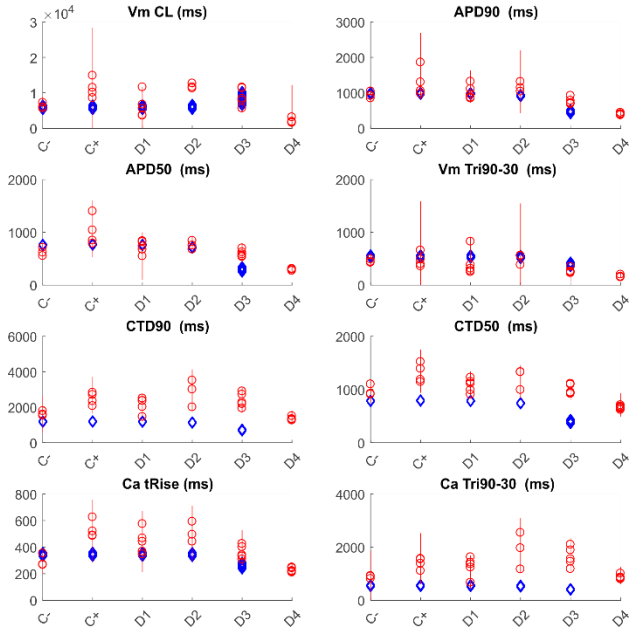

Figure 2. Diltiazem (D1, D2, D3, D4) and Dofetilide (C+) effects on the biomarkers, compared to control (C-). Red circles represent the experimentally recorded biomarkers, and the red bars the experimental variability intervals, for each dose. Blue diamonds are the simulated biomarkers.

D1, D2, D3 and D4 of the plate-specific drugs (Diltiazem was not simulated at D4). The population biomarkers are perfectly included within the experimental variability ranges for C-, thanks to the calibration process. However, drug simulations (D1, D2, D3 and D4) are also in agreement with the drug-induced changes observed in the experiment, although these experiments were not used for the optimization process. For example, Diltiazem shortens APD_{90} and reduces Vm Tri90-30. Conversely, Cisapride and Astemizole prolong APD_{90} and CTD_{90}, increase Ca tRise and the triangulation of both AP and CaTr.

4. Conclusions

In this work we proposed a proof-of-concept optimization of *in silico* populations by means of MoGAs. We observed in particular that by optimizing an *in silico* population on the control experiments of different plates, we then obtain qualitative agreement between simulated and experimental drug effects, without using for a following optimization the experimentally recorded data on the same plate after drug administration. However, for some of the biomarkers, e.g. APD_{50} and APD_{30}, for all the three drugs, especially at the highest drug doses, the simulated drug effects look amplified compared to experiments, possibly due to non-specific and/or multi-channel drug effects experimentally that are not reflected in the model. This work therefore

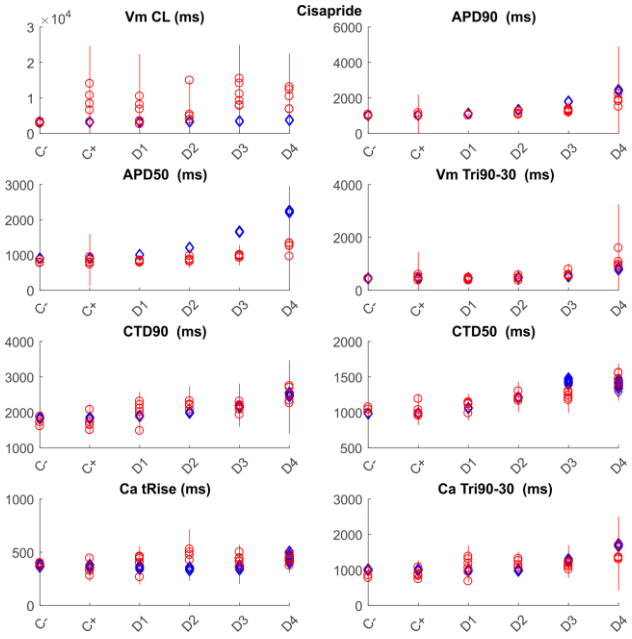

Figure 3. Cisapride (D1, D2, D3, D4) and Dofetilide (C+) effects on the biomarkers, compared to control (C-). Red circles represent the experimentally recorded biomarkers, and the red bars the experimental variability intervals, for each dose. Blue diamonds are the simulated biomarkers.

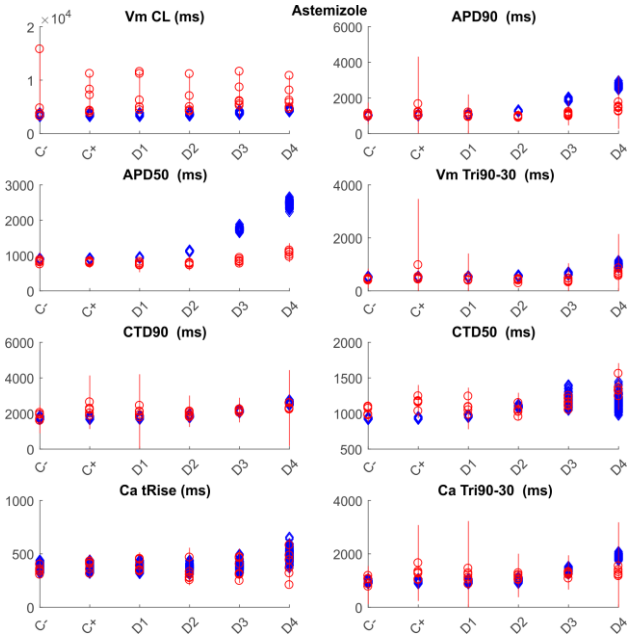

Figure 4. Astemizole (D1, D2, D3, D4) and Dofetilide (C+) effects on the biomarkers, compared to control (C-). Red circles represent the experimentally recorded biomarkers, and the red bars the experimental variability intervals, for each dose. Blue diamonds are the simulated biomarkers.

shows that optically-obtained data are suitable for tuning populations of *in silico* models of hiPSC-CMs and that MoGAs represent an alternative, or can be combined, to canonical approaches for generating populations of *in silico* models.

Acknowledgements

Dr. Michelangelo Paci was supported by the Academy of Finland (decision number 307967). The authors also thank CSC - IT Centre for Science (Finland) and ARC - Advanced Research Computing of University of Oxford (UK) for generous computational resources.

References

[1] Klimas A et al. OptoDyCE as an automated system for high-throughput all-optical dynamic cardiac electrophysiology. Nat Commun. 2016;7(May):11542.

[2] Entcheva E et al. All-optical control of cardiac excitation: Combined high-resolution optogenetic actuation and optical mapping. J Physiol. 2016;9(November 2014):2503–10.

[3] Paci M et al. Automatic optimization of an in silico model of human iPSC derived cardiomyocytes recapitulating calcium handling abnormalities. Front Physiol. 2018;9(June):709.

[4] O'Hara T et al. Simulation of the undiseased human cardiac ventricular action potential: model formulation and experimental validation. PLoS Comput Biol. 2011;7(5):e1002061.

[5] ten Tusscher KHWJ et al. A model for human ventricular tissue. Am J Physiol Hear Circ Physiol. 2004;286(4):H1573-1589.

[6] Stieber J et al. channels: Hyperpolarization-activated, cyclic nucleotide-gated (HCN) channels: from genes to function. In: Cardiac Electrophysiology: From Cell to Bedside. 5th ed. Elsevier; 2009. p. 1184.

[7] Mauerhöfer M et al. Effects of Temperature on Heteromeric Kv11.1a/1b and Kv11.3 Channels. Biophys J. 2016;111(3):504–23.

[8] Paci M et al. Phenotypic variability in LQT3 human induced pluripotent stem cell-derived cardiomyocytes and their response to antiarrhythmic pharmacologic therapy: An in silico approach. Hear Rhythm. 2017;14(11):1704–12.

[9] Paci M et al. A population of in silico models to face the variability of human induced pluripotent stem cell-derived cardiomyocytes: the hERG block case study. In: Computing in Cardiology. 2016. p. 1189–92.

[10] Konak A et al. Multi-objective optimization using genetic algorithms: A tutorial. Reliab Eng Syst Saf. 2006;91(9):992–1007.

[11] Crumb WJ et al. An evaluation of 30 clinical drugs against the comprehensive in vitro proarrhythmia assay (CiPA) proposed ion channel panel. J Pharmacol Toxicol Methods. 2016;

Address for correspondence.

Michelangelo Paci
Tampere University of Technology, BioMediTech
Arvo Ylpön katu 34, D 219, FI-33520 Tampere, Finland
michelangelo.paci@tut.fi